Bidirectional Texture Function Simultaneous Autoregressive Model

Michal Haindl and Michal Havlíček

Institute of Information Theory and Automation
of the ASCR, Prague, Czech Republic
{haindl,havlimi2}@utia.cz

Abstract. The Bidirectional Texture Function (BTF) is the recent most advanced representation of visual properties of surface materials. It specifies their altering appearance due to varying illumination and viewing conditions. Corresponding huge BTF measurements require a mathematical representation allowing simultaneously extremal compression as well as high visual fidelity. We present a novel Markovian BTF model based on a set of underlying simultaneous autoregressive models (SAR). This complex but efficient BTF-SAR model combines several multispectral band limited spatial factors and range map sub-models to produce the required BTF texture space. The BTF-SAR model enables very high BTF space compression ratio, texture enlargement, and reconstruction of missing unmeasured parts of the BTF space.

Keywords: BTF, texture analysis, texture synthesis, data compression, virtual reality.

1 Introduction

Realistic virtual scenes requires object faces covered with synthetic textures visually as close as possible to the corresponding real surface materials they imitate. Such textures have to model rugged surfaces, do not obey Lambertian law, and their reflectance is illumination and view angle dependent. Their most advanced recent representation is the Bidirectional Texture Function (BTF) [3,7,17] which is a 7-dimensional function describing surface texture appearance variations due to varying illumination and viewing angles. Such a function is typically represented by thousands of images per material sample, each taken for a specific combination of the illumination and viewing condition. Visual textures can be either represented by digitised natural textures or textures synthesised from an appropriate mathematical model.

The former simplistic alternative suffers among others with extreme memory requirements for storage of a large number of digitised cross sectioned slices through different material samples or measured BTF space (apposite example can be found in [21]). Sampling solution become even unmanageable for correctly modeled visual scenes with BTF texture representation which require to store tens thousands of different illumination and view angle samples for every texture

E. Salerno, A.E. Çetin, and O. Salvetti (Eds.): MUSCLE 2011, LNCS 7252, pp. 149–159, 2012.

so that even simple visual scene with several materials requires to store tera bytes of texture data which is still far out of limits for any current and near-future hardware. Several intelligent sampling methods (for example [4,5] and many others) were proposed to reduce these extreme memory requirements. All these methods are based on some sort of original small texture sampling and the best of them produce very realistic synthetic textures. However they require to store thousands images for every combination of viewing and illumination angle of the original target texture sample and in addition often produce visible seams (except for method presented in [13]). Some of them are computationally demanding and they are not able to generate textures unseen [17] by these algorithms.

Contrary to the sampling approaches, the synthetic textures generated from mathematical models are more flexible and extremely compressed, because several parameters have to be stored only. They may be evaluated directly in a procedural form and can be used to fill virtually infinite texture space without visible discontinuities. On the other hand, mathematical models can only approximate real measurements, which results in visual quality compromise for some oversimplified methods. Several multispectral smooth modelling approaches were published - consult for example [9,15,1,18,16,12,11]. Modelling static BTF textures requires seven dimensional models, but it is possible to approximate this general BTF model with a set of much simpler three or two dimensional factorial models, provided we will accept some information loss.

Among such possible models the random fields are appropriate for texture modelling not only because they do not suffer from some problems of alternative options (see [9,18] for details), but they also provide easy texture synthesis and sufficient flexibility to reproduce a large set of both natural and artificial textures. While the random field based models quite successfully represent high frequencies present in natural textures, low frequencies are sometimes difficult for them. This slight drawback may be overcome by using a multiscale random field model. Multiple resolution decomposition such as Gaussian Laplacian pyramids, wavelet pyramids or subband pyramids present efficient method for the spatial information compressing. The hierarchy of different resolutions of an input image provides a transition between pixel level features and region or global features and hence such a representation simplify modelling a large variety of possible textures. Each resolution component is both analysed and synthesised independently.

We propose a novel algorithm for efficient rough texture modelling which combines an estimated range map with synthetic multiscale SAR based generated smooth texture. The texture visual appearance during changes of viewing and illumination conditions are simulated using the bump mapping [2] or displacement mapping [22] technique. The obvious advantage of this solution is the possibility to use hardware support for both bump and displacement mapping techniques in the contemporary visualisation hardware (GPU).

2 BTF-SAR Model

The BTF-SAR model combines an estimated range map with synthetic multiscale smooth texture. The overall BTF-SAR model scheme is on Fig.1. The model starts with range map estimation (section 2.1) followed by the BTF illumination / view $(\theta_i, \phi_i/\theta_v, \phi_v)$ space segmentation into c subspace images (the closest BTF images to cluster centers) using the K-means algorithm. Eigen-analysis of BTF data has shown that $c = 20$ is sufficient to represent its reflectance correctly for most of the material samples. The color cumulative histograms of individual BTF images, in perceptually uniform CIE Lab color-space, are used as the data features. Smooth parts of single BTF subspace spatial factors (section 2.2) textures $(3D\ Y)$ are modelled using the SAR factorial texture model of section 3. Each multispectral fine-resolution BTF subspace component is obtained from the pyramid collapse procedure (i.e. the interpolation of sub-band components - the inversion process to the creation of the Gaussian-Laplacian pyramid).

The overall BTF texture visual appearance during changes of viewing and illumination conditions is simulated using either bump or displacement mapping technique. This solution can benefit from bump / displacement mapping hardware support in contemporary visualisation hardware.

Let us denote multiindices r, s $r = (r_1, r_2)$, $r \in I$ or $r \in \tilde{I}$, (similarly for $s = (s_1, s_2)$) where $I, \tilde{I}$ are discrete 2-dimensional finite rectangular lattices with toroidal border conditions indexing the model random field and measured BTF images, respectively. Usually, the synthesized random field is much larger than the measured one, i.e. $\tilde{I} \subset I$. r_1 is the row, and r_2 the column index, respectively. Y_r is multispectral pixel at location r and $Y_{r,j} \in \mathcal{R}$ is its j-th spectral plane component $(j \in <1; d>)$.

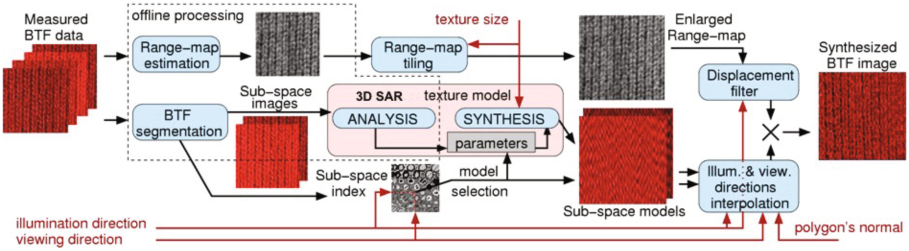

Fig. 1. The BTF-SAR modelling scheme

2.1 Range Map Modelling

The overall roughness of a textured surface significantly influences the BTF texture appearance. Such a surface can be specified using its single range map per material, which can be either measured or estimated by several existing approaches such as the shape from shading [8], shape from texture [6] or photometric stereo [23], respectively. The BTF-SAR range map estimate benefits from tens of ideally mutually registered BTF measurements (e.g. 81 for a fixed view of the University of Bonn data) and uses the over-determined photometric stereo from mutually aligned BTF images. The estimated material range map is further enlarged by the image roller technique [13,14]. The photometric stereo enables to acquire the normal and albedo fields from at least three intensity images obtained for different illuminations but fixed camera position while a Lambertian opaque surface is assumed. However, the photometric stereo method is not well suited for surfaces with highly specular reflectance, highly subsurface scattering or strong occlusion, since it breaks the underlying Lambertain reflectance assumption.

2.2 Spatial Factorization

An analysed BTF subspace texture is decomposed into multiple resolutions factors using the Laplacian pyramid and the intermediary Gaussian pyramid $\ddot{Y}_{\bullet}^{(k)}$ which is a sequence of images in which each one is a low-pass down-sampled version of its predecessor. The symbol $\bullet$ denotes all corresponding indices $(\forall r \in I)$. The Gaussian pyramid for a reduction factor n is [11]:

$$Y_r^{''(k)} = \downarrow_r^n (Y_{\bullet,i}^{''(k-1)} \otimes w) \quad k = 1, 2, \ldots , \tag{1}$$

$\downarrow_r^n$ denotes down-sampling with reduction factor n and $\otimes$ is the convolution operation. The Laplacian pyramid $Y_r^{'(k)}$ contains band pass components and provides a good approximation to the Laplacian of the Gaussian kernel. It can be constructed by differencing single Gaussian pyramid layers:

$$Y_r^{'(k)} = Y_r^{''(k)} - \uparrow_r^n (Y_{\bullet}^{''(k+1)}), \quad k = 0, 1, \ldots . \tag{2}$$

Each resolution data are independently modelled by their dedicated SAR.

3 SAR Factorial Texture Model

Single multispectral smooth texture factors are modelled using the multispectral simultaneous autoregressive model (SAR) [1]. The 3D SAR model relates each zero mean pixel value Y_r by a linear combination of neighbouring pixel values and an additive uncorrelated Gaussian noise component[1]:

$$Y_{r,i} = \sum_{j=1}^{d} \sum_{s \in I_r^{i,j}} a_{s,i,j} \, Y_{r \oplus s,j} + e_{r,i}, \qquad i = 1, \ldots, d \ , \tag{3}$$

where d equals the number of image spectral planes, $I_r^{i,j}$ denotes the neighbour set relating pixels in plane i to neighbouring ones in plane j, $a_{s,i,j}$, $s \in I_r$ are the corresponding parameters which define the dependence of $Y_{r,i}$ on its neighbour sets $I_r^{i,j}$ $\forall j$. The driving Gaussian noise $e_{r,i}$ are i.i.d. random variables with zero mean and the $i-$th spectral plane variance is denoted σ_i. The symbol

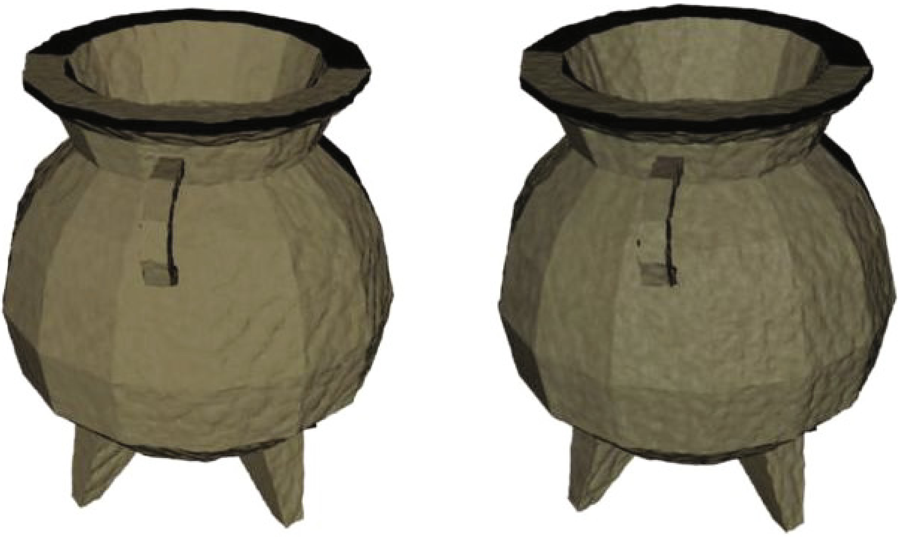

Fig. 2. Synthetic leather (left) and foil mapped to the kettle object

$\oplus$ denotes modulo M addition in each index. Note that the SAR model can be easily defined also for other than the Gaussian noise.

Rewriting the autoregressive equation (3) to the matrix form for the multispectral model, i.e., $i \in \{1, \ldots, d\}$, the SAR model equations are

$$\Psi Y = \epsilon \tag{4}$$

where

$$\Psi = \begin{pmatrix} \Psi_{11} & \Psi_{12} & \ldots & \Psi_{1d} \\ \Psi_{21} & \Psi_{22} & \ldots & \Psi_{2d} \\ \vdots & \vdots & & \vdots \\ \Psi_{d1} & \Psi_{d2} & \ldots & \Psi_{dd} \end{pmatrix} , \tag{5}$$

$$Y = [Y_{[1]}, Y_{[2]}, \ldots, Y_{[d]}]^T \ ,$$
$$\epsilon = [e_{[1]}, e_{[2]}, \ldots, e_{[d]}]^T \ ,$$

and both $Y_{[i]}$ and $e_{[i]}$ are M^2 vectors of lexicographic ordered arrays $\{Y_{\bullet,i}\}$ and $\{e_{\bullet,i}\}$. The transformation matrix Ψ is composed of $M^2 \times M^2$ block circulant submatrices (6):

$$\Psi_{ij} = \begin{pmatrix} \Psi_{ij}^{1} & \Psi_{ij}^{2} & \ldots & \Psi_{ij}^{M} \\ \Psi_{ij}^{M} & \Psi_{ij}^{1} & \ldots & \Psi_{ij}^{M-1} \\ \vdots & \vdots & \ddots & \vdots \\ \Psi_{ij}^{2} & \Psi_{ij}^{3} & \ldots & \Psi_{ij}^{1} \end{pmatrix} \tag{6}$$

where each Ψ^k_{ij} is a $M \times M$ circulant matrix whose (m,n)-th element is given by:

$$\Psi^k_{ij,m,n} = \begin{cases} 1, & i=j,\; m=n,\; k=1, \\ -a_{s,i,j}, & s_1 = k-1, \quad s_2 = ((n-m) \mod M),\; (s_1,s_2) \in I^{ij}_r, \\ 0, & \textit{otherwise}. \end{cases} \tag{7}$$

Writing the image observations (4) as

$$Y = \Psi^{-1}\,\epsilon \ ,$$

the image covariance matrix is obtained as

$$\Sigma_Y = E\{YY^T\} = E\left\{\Psi^{-1}\epsilon\,\epsilon^T\Psi^{-T}\right\} = \Psi^{-1}\Sigma_\epsilon\,\Psi^{-T}$$

where

$$\Sigma_\epsilon = E\{\epsilon\epsilon^T\} = \begin{pmatrix} \sigma_1 I & 0 & \dots & 0 \\ 0 & \sigma_2 I & \dots & 0 \\ \vdots & & & \vdots \\ 0 & 0 & \dots & \sigma_d I \end{pmatrix} . \tag{8}$$

3.1 Parameter Estimation

The selection of an appropriate SAR model support is important to obtain good results in modelling of a given random field. If the contextual neighbourhood is too small, it cannot capture all details of the random field. Contrariwise, inclusion of the unnecessary neighbours adds to the computational burden and can potentially degrade the performance of the model as an additional source of noise. Direct selection of the optimal support requires numerical optimization hence we exploit a spatial correlation approach [15]. Similarly, both Bayesian as well as the maximum likelihood SAR parameter estimators require numerical optimization.

A least squares (LS) SAR model parameters estimate allows to avoid an expensive numerical optimization method at the cost of accuracy. It can be obtained by equating the observed pixel values of an image to the expected value of the model equations. For a multispectral SAR model this task leads to d independent systems of M^2 equations:

$$\begin{aligned} Y_{r,i} &= E\left\{Y_{r,i}\,|\,\gamma_i\right\} = X^T_{r,i}\,\gamma_i, \qquad\qquad r \in I,\; i \in \{1,\dots,d\} \ , \\ \gamma_i &= \left[\gamma_{i1},\gamma_{i2},\dots,\gamma_{id}\right]^T \ , \\ X_{r,i} &= \left[\{Y_{r\oplus s,1} : s \in I^{i1}_r\},\, \{Y_{r\oplus s,2} : s \in I^{i2}_r\},\dots,\{Y_{r\oplus s,d} : s \in I^{id}_r\}\right]^T \ , \end{aligned} \tag{9}$$

where $\gamma_{ij} = [a_{s,i,j} : \forall s \in I^{i,j}_r]$ and for which the LS estimates $\hat{\gamma_i}$ and $\hat{\sigma_i}$ can be found as

$$\hat{\gamma}_i = \left(\sum_{s \in I} X_{s,i}\, X_{s,i}^T \right)^{-1} \left(\sum_{s \in I} X_{s,i}\, Y_{s,i} \right) \;,$$

$$\hat{\sigma_i} = \frac{1}{M^2} \sum_{s \in I} \left(Y_{s,i} - \hat{\gamma_i}^T X_{s,i} \right)^2 \;.$$

3.2 SAR Model Synthesis

A general multidimensional SAR model has to be synthesized using some of the Markov Chain Monte Carlo (MCMC) methods. Due to our toroidal lattice assumption we can use a noniterative efficient synthesis which uses the discrete fast Fourier transformation (DFT) instead. The SAR model equations (3) may be expressed in terms of the DFT of each image plane as:

$$\tilde{Y}_{t,i} = \sum_{j=1}^{d} \sum_{s \in I_r^{ij}} a_{s,i,j}\, \tilde{Y}_{t,j}\, e^{\sqrt{-1}\omega_{st}} + \tilde{\epsilon}_{t,i}, \qquad i = 1, \ldots, d, \tag{10}$$

where $\tilde{Y}_{t,i}$ and $\tilde{\epsilon}_{t,i}$ are the 2D DFT coefficients of the image observation and noise sequences $\{Y_{s,i}\}$ and $\{e_{s,i}\}$, respectively, at discrete frequency index $t = (m,n)$ and $\omega_{rt} = \frac{2\pi(mr_1+nr_2)}{M}$. For the multispectral model this can be written in matrix form as

$$\tilde{Y}_t = \Lambda_t^{-1}\, \Sigma^{\frac{1}{2}}\, \tilde{\epsilon}_t, \qquad t \in I, \tag{11}$$

where

$$\tilde{Y}_t = [\tilde{Y}_{t,1}, \tilde{Y}_{t,2}, \ldots, \tilde{Y}_{t,d}]^T \;,$$
$$\tilde{\epsilon}_t = (\tilde{\epsilon}_{t,1}, \tilde{\epsilon}_{t,2}, \ldots, \tilde{\epsilon}_{t,d})^T \;,$$

$$\Sigma^{\frac{1}{2}} = \begin{pmatrix} \sqrt{\sigma_1} & 0 & \ldots & 0 \\ 0 & \sqrt{\sigma_2} & \ldots & 0 \\ \vdots & & & \vdots \\ 0 & 0 & \ldots & \sqrt{\sigma_d} \end{pmatrix} \;,$$

$$\Lambda_t = \begin{pmatrix} \lambda_{t,11} & \lambda_{t,12} & \ldots & \lambda_{t,1d} \\ \lambda_{t,21} & \lambda_{t,22} & \ldots & \lambda_{t,2d} \\ \vdots & & & \vdots \\ \lambda_{t,d1}(t) & \lambda_{t,d2} & \ldots & \lambda_{t,dd} \end{pmatrix} \;,$$

$$\lambda_{t,ij} = \begin{cases} 1 - \sum_{s \in I_r^{ij}} a_{s,i,j}\, e^{\sqrt{-1}\omega_{st}} & i = j \;, \\ - \sum_{s \in I_r^{ij}} a_{s,i,j}\, e^{\sqrt{-1}\omega_{st}} & i \neq j \;. \end{cases}$$

The SAR model is stable and valid if Λ_t is non-singular matrix $\forall t \in I$. Given the estimated model parameters, a $d \times M \times M$ multispectral SAR image can be non iteratively synthesized using the following algorithm:

1. Generate the i.i.d. noise arrays $\{e_{r,i}\}$ for each image plane using a Gaussian random number generator.
2. Calculate the 2D DFT of each noise array, i.e., produce the transformed noise arrays $\{\tilde{e}_{t,i}\}$.
3. For each discrete frequency index t, compute $\tilde{Y}_t = \Lambda_t^{-1} \, \Sigma^{\frac{1}{2}} \, \tilde{e}_t$.
4. Perform the 2D inverse DFT of each frequency plane $\{\tilde{Y}_{t,i}\}$, producing the synthesized image planes $\{Y_{s,i}\}$.

The resulting image planes will have zero mean thus it is necessary to add the estimated mean to each spectral plane in the end. The fine resolution texture is obtained from the pyramid collapse procedure (inversion process to process described in section 2.2).

4 Results

We have tested the BTF-SAR model algorithm on BTF colour textures from the University of Bonn BTF measurements [17,21] (among several available materials are leather, wood, or wool). Each BTF material sample comprised in the University of Bonn database is measured in 81 illumination and 81 viewing angles and has resolution 800 × 800 pixels, so that 81 × 81 images had to be analysed for each material. Fig.2 demonstrates the synthesised result for leather and foil materials, i.e. synthesised BTF textures combined with their range maps in the displacement mapping filter of the rendering Blender[1] software with the

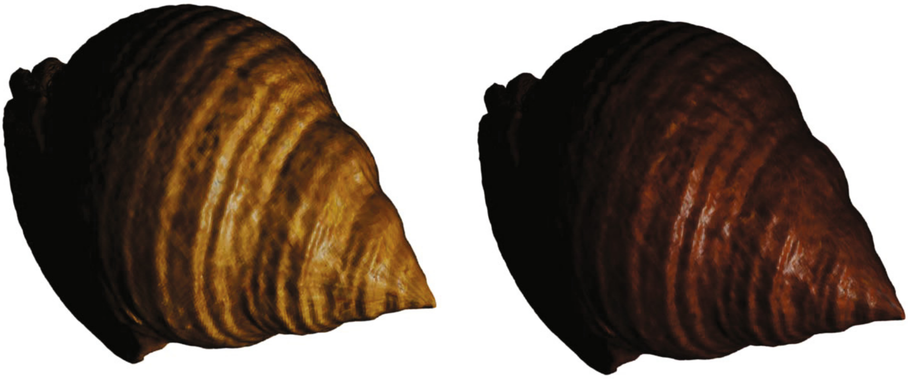

Fig. 3. Two types of modelled wood textures mapped to the conch model

[1] www.blender.org

BTF plugin [19,20] and mapped to the kettle model[2] The scene was rendered in several different illumination conditions to demonstrate visual quality of the synthesised BTF. The same approach for two different wood varieties and a detailed conch model measured using our Konika-Minolta laser scanner is illustrated on Fig.3.

Table 1. Mutual comparison of 3D Gaussian Markovian models, PC with 2 Dual Core Pentium 2.8 GHz CPU time was tested using the symmetric half of the first order hierarchical neighbourhood (i.e. 3 neighbours) on 800 × 800 training and 512 × 512 synthesized texture, respectively

	Properties			
model	Markovianity	analysis	synthesis	support
SAR	wide-sense	approx.	MCMC / FFT	general
CAR	wide-sense	analytical	analytical	causal / unilateral
GMRF	strict-sense	approx.	MCMC / FFT	symm. hierarchical

		CPU time [s]	
model	stability	analysis	synthesis
SAR	+	0.25	1.35
CAR	−	0.55	0.15
GMRF	+	3.9	2.5

Tab.1 surveys the basic features of three related SAR, CAR [12], GMRF [10] factorial texture models which can alternate in the overall BTF model. All these 3D models can be expressed in the autoregressive form but only the CAR model can be solved analytically [12], does not require the toroidal border assumption, and has by the order of magnited faster synthesis. However, both non causal models (SAR, GMRF) are more general and robust. Analogous conclusions hold also for their 2D counterparts.

5 Conclusion

Our testing results of the algorithm on all available BTF data are promising although they are based on the mathematical model in contrast to the intelligent sampling approach, and as such they can only approximate realism of the original measurement. Some synthetic textures reproduce given measured texture images so that both natural and synthetic textures are almost visually indiscernible. Even the not so successful results can be used for the preattentive BTF textures applications. The main benefit of this inherently multispectral method is more realistic representation of texture colourfulness, which is naturally apparent in

[2] `http://e2-productions.com/repository/modules/PDdownloads/singlefile.php?cid=10&lid=388`

case of very distinctively coloured textures. The multi scale approach is more robust and sometimes allows better results than the singlescale one.

The presented BTF-SAR model offers fast seamless enlargement of BTF texture to arbitrary size, very high BTF texture compression ratio which cannot be achieved by any other sampling based BTF texture synthesis method. This is advantageous for transmission, storing or modelling visual surface texture data while the model has still moderate computation complexity. The method does not need any time consuming numerical optimisation like the usually employed Markov chain Monte Carlo method or some of their deterministic approximation. In addition, this model may be used to reconstruct BTF space (i.e. missing parts of the BTF measurement space) or even non existing (i.e. previously not measured or edited) BTF textures. The model is also potentially capable of direct implementation inside the graphical card processing unit or a multithreaded implementation.

Acknowledgements. This research was supported by the grant GAČR 102/08/0593 and partially by the projects MŠMT 1M0572 DAR, GAČR 103/11/0335, CESNET 387/2010.

References

1. Bennett, J., Khotanzad, A.: Multispectral random field models for synthesis and analysis of color images. IEEE Trans. on Pattern Analysis and Machine Intelligence 20(3), 327–332 (1998)
2. Blinn, J.: Simulation of wrinkled surfaces. SIGGRAPH 1978 12(3), 286–292 (1978)
3. Dana, K.J., Nayar, S.K., van Ginneken, B., Koenderink, J.J.: Reflectance and texture of real-world surfaces. In: CVPR, pp. 151–157. IEEE Computer Society (1997)
4. De Bonet, J.: Multiresolution sampling procedure for analysis and synthesis of textured images. In: ACM SIGGRAPH 1997, pp. 361–368. ACM Press (1997)
5. Efros, A.A., Freeman, W.T.: Image quilting for texture synthesis and transfer. In: Fiume, E. (ed.) ACM SIGGRAPH 2001, pp. 341–346. ACM Press (2001), `citeseer.nj.nec.com/efros01image.html`
6. Favaro, P., Soatto, S.: 3-D shape estimation and image restoration: exploiting defocus and motion blur. Springer-Verlag New York Inc. (2007)
7. Filip, J., Haindl, M.: Bidirectional texture function modeling: A state of the art survey. IEEE Transactions on Pattern Analysis and Machine Intelligence 31(11), 1921–1940 (2009)
8. Frankot, R.T., Chellappa, R.: A method for enforcing integrability in shape from shading algorithms. IEEE Trans. on Pattern Analysis and Machine Intelligence 10(7), 439–451 (1988)
9. Haindl, M.: Texture synthesis. CWI Quarterly 4(4), 305–331 (1991)
10. Haindl, M., Filip, J.: Fast BTF texture modelling. In: Chantler, M. (ed.) Proceedings of Texture 2003, pp. 47–52. IEEE Press, Edinburgh (2003)
11. Haindl, M., Filip, J.: A Fast Probabilistic Bidirectional Texture Function Model. In: Campilho, A.C., Kamel, M.S. (eds.) ICIAR 2004, Part II. LNCS, vol. 3212, pp. 298–305. Springer, Heidelberg (2004)

12. Haindl, M., Filip, J., Arnold, M.: BTF image space utmost compression and modelling method. In: Kittler, J., Petrou, M., Nixon, M. (eds.) Proceedings of the 17th IAPR International Conference on Pattern Recognition, vol. III, pp. 194–197. IEEE, Los Alamitos (2004), http://dx.doi.org/10.1109/ICPR.2004.1334501
13. Haindl, M., Hatka, M.: BTF Roller. In: Chantler, M., Drbohlav, O. (eds.) Proceedings of the 4th International Workshop on Texture Analysis, Texture 2005, pp. 89–94. IEEE, Los Alamitos (2005)
14. Haindl, M., Hatka, M.: A roller - fast sampling-based texture synthesis algorithm. In: Skala, V. (ed.) Proceedings of the 13th International Conference in Central Europe on Computer Graphics, Visualization and Computer Vision, pp. 93–96. UNION Agency - Science Press, Plzen (2005)
15. Haindl, M., Havlíček, V.: Multiresolution colour texture synthesis. In: Dobrovodský, K. (ed.) Proceedings of the 7th International Workshop on Robotics in Alpe-Adria-Danube Region, pp. 297–302. ASCO Art, Bratislava (1998)
16. Haindl, M., Havlíček, V.: A multiscale colour texture model. In: Kasturi, R., Laurendeau, D., Suen, C. (eds.) Proceedings of the 16th International Conference on Pattern Recognition, pp. 255–258. IEEE Computer Society, Los Alamitos (2002), http://dx.doi.org/10.1109/ICPR.2002.1044676
17. Haindl, M., Filip, J.: Advanced textural representation of materials appearance. In: SIGGRAPH Asia 2011 Courses, SA 2011, pp. 1:1–1:84. ACM, New York (2011), http://doi.acm.org/10.1145/2077434.2077435
18. Haindl, M., Havlícek, V.: A Multiresolution Causal Colour Texture Model. In: Amin, A., Pudil, P., Ferri, F., Iñesta, J.M. (eds.) SPR 2000 and SSPR 2000. LNCS, vol. 1876, pp. 114–122. Springer, Heidelberg (2000)
19. Hatka, M.: Btf textures visualization in blender. In: Proceedings of the Graduate Students Days, pp. 37–46. FNSPE CTU (2009)
20. Hatka, M., Haindl, M.: Btf rendering in blender. In: Zhang, X., Pan, Z., Dong, W., Liu, Z.Q. (eds.) Proceedings of the 10th International Conference on Virtual Reality Continuum and Its Applications in Industry, VRCAI 2011, pp. 265–272. ACM, New York (2011), http://doi.acm.org/10.1145/2087756.2087794
21. Müller, G., Meseth, J., Sattler, M., Sarlette, R., Klein, R.: Acquisition, synthesis and rendering of bidirectional texture functions. In: Eurographics 2004. STAR - State of The Art Report, pp. 69–94. Eurographics Association (2004)
22. Wang, L., Wang, X., Tong, X., Lin, S., Hu, S., Guo, B., Shum, H.: View-dependent displacement mapping. ACM Transactions on Graphics 22(3), 334–339 (2003)
23. Woodham, R.: Photometric method for determining surface orientation from multiple images. Optical Engineering 19(1), 139–144 (1980)